Comput Geosci
DOI 10.1007/s10596-017-9619-2

ORIGINAL PAPER

Downscaling the 2D Bénard convection equations using continuous data assimilation

M. U. Altaf[1] · E. S. Titi[2] · T. Gebrael[3] · O. M. Knio[1] · L. Zhao[4] · M. F. McCabe[1] · I. Hoteit[1]

Received: 22 December 2015 / Accepted: 19 January 2017

Abstract We consider a recently introduced continuous data assimilation (CDA) approach for downscaling a coarse resolution configuration of the 2D Bénard convection equations into a finer grid. In this CDA, a nudging term, estimated as the misfit between some interpolants of the assimilated coarse-grid measurements and the fine-grid model solution, is added to the model equations to constrain the model. The main contribution of this study is a performance analysis of CDA for downscaling measurements of temperature and velocity. These measurements are assimilated either separately or simultaneously, and the results are compared against those resulting from the standard point-to-point nudging approach (NA). Our numerical results suggest that the CDA solution outperforms that of NA, always converging to the true solution when the velocity is assimilated as has been theoretically proven. Assimilation of temperature measurements only may not always recover the true state as demonstrated in the case study. Various runs are conducted to evaluate the sensitivity of CDA to noise in the measurements, the size, and the time frequency of the measured grid, suggesting a more robust behavior of CDA compared to that of NA.

✉ I. Hoteit
ibrahim.hoteit@kaust.edu.sa

[1] King Abdullah University of Science and Technology, Thuwal, Saudi Arabia

[2] Department of Mathematics, Texas A&M University, College Station, TX 77843, USA

[3] American University of Beirut, Beirut, Lebanon

[4] Georgia Institute of Technology, Atlanta, GA, USA

Keywords Continuous data assimilation · Bénard convection equations · Dynamical downscaling

1 Introduction

An important use of present-day numerical models is to provide accurate predictions of physical phenomena from a known present state and some prior information. In some cases, the output from these numerical models is often too spatially coarse to be used directly to assess particular local phenomena (e.g., climate models). In order to improve the representation of local-scale processes, downscaling techniques can be applied. Downscaling methods are needed to obtain local-scale weather and climate, based on regional-scale atmospheric (and oceanic) variables that are provided by global circulation models (GCMs). Two basic approaches are followed in downscaling: (i) statistical downscaling and (ii) dynamical downscaling.

In the statistical downscaling (SD), an empirical relationship is established from observations between large-scale variables and a local variable at a particular station. The relationship is then used to estimate the local variables from the coarse global fields [1–4]. A review of SD methods can be found in [5]. The dynamical downscaling (DD) on the other hand fits regional circulation models (RCMs) into outputs from GCMs [6]. The nudging algorithm is one of the standard methods in DD, which basically forces RCM simulations toward large-scale driving data point-to-point. A number of studies have examined the performance of nudging in reanalysis-driven RCM simulations (e.g., [7, 8]). These RCM simulations for instance show better temporal variations of precipitation relative to those without nudging [9]. Various studies demonstrated that the overall performance of SD and DD was comparable in reproducing the

Published online: 27 February 2017

present-day climate for the respective regions [10, 11]. It is generally more straightforward and physically consistent to use the dynamical information when available, rather than a statistical model, to downscale global fields.

The study of different geophysical processes is based on both modeling and observations of the dynamical model state. None of the two disciplines has proved to be more useful. Instead both disciplines take advantage of each other. Observational data usually serve to validate numerical models, and observations are interpolated in space and time using the models. Data assimilation (DA) is the technique that merges these two sources into a single product. The basic idea of DA is to regularly update a numerical model with observational data [12–14]. Given a sufficiently realistic numerical model and reliable observations, the joint product provides an estimate of the state of the ocean or atmosphere that should be better than the respective single sources. Apart from the quality of the model or the observations, the success of DA depends on how well the two sources are combined.

Continuous data assimilation (CDA) methods incorporate observational data directly into the model equations as the model is being integrated in time [15, 16]. One way to achieve this is by introducing low-Fourier-mode observables into the model equations for the evolution of high Fourier modes [17–21]. Recently, a new approach to CDA was introduced in [22] based on ideas from control theory. Instead of inserting the measurements directly into the model, in this CDA approach, a nudging term, estimated as the misfit between some interpolants of the assimilated coarse-grid measurements and the fine-grid model solution, is added to the model equations to constrain the model large-scale variability by available measurements. This new CDA approach was designed for general dissipative dynamical systems, and has been theoretically analyzed in different scenarios [23–25] and recently tested numerically on the two-dimensional incompressible Navier-Stokes equations in [26].

In this paper, CDA is examined for downscaling a coarse-scale solution of the non-linear 2D Bénard convection problem (a Boussinesq system between two solid plates, heated from the bottom and cooled from the top). The Bénard convection equations solve the reduced form of Navier-Stokes equations coupled with temperature and are one of the classical problems in the heat transfer literature [31]. This is the first application of CDA in a stratified flow. The coarse mesh data is generated for temperature and velocity. The CDA algorithm is then applied to downscale these variables, assimilating temperature observations, velocity observations, or both. The CDA results are then compared with the standard nudging approach (NA), showing that CDA is more performant and more robust than NA [30]. We also study the performance of CDA with respect to noise in the assimilated observations, time frequency of observations, the number of observation points, and different choices of interpolants. Our results suggest that the CDA method is a fast and accurate approach with favorable robustness properties for the dynamical downscaling of the 2D Bénard convection equations.

The CDA algorithm in [22] has been theoretically investigated in [27] for the 2D Bénard convection through velocity measurements alone, with a finding that velocity measurements alone are enough to construct the approximate solutions for both velocity and temperature. An earlier study by Charney et al. [15] claimed that the temperature measurements are enough to determine all other variables in the atmosphere. Ghil et al. [28, 29] showed that this was only true for some simple models, but gave other numerical tests showing that this is not always true. We present and analyze the case where temperature does not necessarily recover the velocity field. This is demonstrated based on an example where assimilation starts from an initial shear flow.

In the next section, a description of the 2D Bénard convection numerical model is given; after which, we briefly describe the CDA technique in Section 3. The numerical results obtained with the 2D Bénard convection model are presented in Section 4 while conclusions are provided in Section 5.

2 Bénard convection problem

Known as the Bénard convection problem, the thermally driven rectangular cavity with adiabatic top and bottom walls is one of the classical problems in the heat transfer literature [31]. It is also one of the most popular test-problems for comparing numerical algorithms. The model equations are cast in dimensionless form using an appropriate scaling of dynamical variables. Using tildes to denote dimensional quantities, we use the cavity height, $\tilde{H}$ as reference length-scale, $V_r \equiv (\tilde{\kappa}/\tilde{H})Ra^{0.5}$ as reference velocity, and the background temperature difference $\tilde{T}_2 - \tilde{T}_1$ as characteristic temperature. Ra denotes the Rayleigh number, whereas $\tilde{\kappa}$ is the thermal conductivity. With the current choice of scaling parameters, the normalized momentum, energy, and mass conservation equations are as follows:

$$\frac{\partial \boldsymbol{u}}{\partial t} + (\boldsymbol{u}\cdot\nabla)\boldsymbol{u} + \nabla p = \frac{Pr}{\sqrt{Ra}}\nabla^2\boldsymbol{u} + Pr\Theta\boldsymbol{e}_2, \tag{1}$$

$$\frac{\partial \Theta}{\partial t} + (\boldsymbol{u}\cdot\nabla)\Theta = \frac{1}{\sqrt{Ra}}\nabla^2\Theta + \boldsymbol{u}\cdot\boldsymbol{e}_2, \tag{2}$$

$$\nabla\cdot\boldsymbol{u} = 0, \tag{3}$$

where $\boldsymbol{u} = (u, v)$ denotes the velocity vector, p is pressure, t is time, $\Theta \equiv (T - 0.5(T_1 + T_2))/(T_2 - T_1)$ is the temperature anomaly, $\boldsymbol{e}_2$ the standard basis vector in the y direction,

and Pr is the Prandtl number. The system is completed by specifying the initial conditions:

$$\boldsymbol{u}(0;(x,y)) = \boldsymbol{u}_0(x,y), \tag{4}$$

and

$$\Theta(0;(x,y)) = \Theta_0(x,y), \tag{5}$$

the boundary conditions and the top and bottom boundaries,

$$\boldsymbol{u} = 0 \text{ at } \ y = 0 \text{ and } \ y = 1,$$

and

$$\Theta = 0 \text{ at } \ y = 0 \text{ and } \ y = 1,$$

and periodicity conditions in x for velocity, temperature, and pressure.

2.1 Numerical solution

The governing equations are simulated using a finite difference methodology. We use a staggered, marker-and-cell (MAC) grid to discretize field variables. Specifically, a Cartesian grid is used, with n_x and n_y cells in the x and y directions, respectively. The corresponding cell sizes are $\Delta x = 1/n_x$ and $\Delta y = 1/n_y$. Temperature and pressure are discretized on cell centers, whereas the velocity components u and v are discretized on vertical and horizontal cell faces, respectively. Gradients are approximated using conservative, second-order, centered differences.

The system of discretized equations is integrated in time using a pressure projection scheme. The pressure-free momentum and energy equations are first integrated in time using a mixed integration approach. The second-order Adams-Bashforth scheme is used for the convective terms, diffusion terms are treated using the Euler backward scheme, whereas the remaining (linear) terms are handled using a first-order explicit Euler scheme. A pressure projection step is then applied in order to satisfy the continuity equation.

3 Downscaling approaches

3.1 Grid nudging method

Suppose the time evolution of $U \equiv (\boldsymbol{u}, \Theta)$ is governed by a given system of the form (1)–(5), mentioned above, where the initial data is not known. We construct an increasingly accurate solution based on coarse-grid data from which predictions of $(\boldsymbol{u}(t), \Theta(t))$ can be made. In the standard NA, the interior solution of the model, denoted as $(\boldsymbol{u}(t), \Theta(t))$, is brought closer to, or "nudged" towards the observations, $\left\{\boldsymbol{u}_j^o, \Theta_j^o\right\}$, $j = 1, \ldots, N$, where N is the number of observation points located at $\boldsymbol{x}_j$, namely by adding an adjustment or restoring term. The velocity nudging term is expressed as follows: $\sum_{j=1}^{N} \alpha_u(\boldsymbol{u}_j^o - \boldsymbol{u}(\boldsymbol{x_j}))\delta(\boldsymbol{x} - \boldsymbol{x}_j)$, where the "nudging coefficient" α_u is tuned to minimize discrepancy; a similar nudging is used for temperature. The updated equations will then be of the form as follows:

$$\frac{\partial \boldsymbol{u}}{\partial t} - \frac{Pr}{\sqrt{Ra}}\nabla^2\boldsymbol{u} + (\boldsymbol{u}\cdot\nabla)\boldsymbol{u} + \nabla p = Pr\Theta\boldsymbol{e}_2 + \sum_{j=1}^{N} \alpha_u(\boldsymbol{u}_j^o - \boldsymbol{u}(\boldsymbol{x_j}))\delta(\boldsymbol{x} - \boldsymbol{x}_j), \tag{6}$$

$$\frac{\partial \Theta}{\partial t} - \frac{1}{\sqrt{Ra}}\nabla^2\Theta + (\boldsymbol{u}\cdot\nabla)\Theta - \boldsymbol{u}\cdot\boldsymbol{e}_2 = \sum_{j=1}^{N} \alpha_\Theta(\Theta_j^o - \Theta(\boldsymbol{x_j}))\delta(\boldsymbol{x} - \boldsymbol{x}_j), \tag{7}$$

$$\nabla\cdot\boldsymbol{u} = 0, \tag{8}$$

with initial conditions:

$$\boldsymbol{u}(0;(x,y)) = 0, \tag{9}$$

$$\Theta(0;(x,y)) = 0. \tag{10}$$

We call the solution (1)–(5) the reference solution, and the solution of (6)–(10) the (NA) estimated solution.

3.2 Continuous data assimilation

In the CDA approach, interpolants are applied on both model outputs and coarse data before nudging, allowing to only constrain the large-scale flow of the model as shown by [22]. Let $I_h(\phi(x))$ be an interpolation operator of a function $\phi(x)$. For instance, one can take

$$I_h(\phi)(x) = \sum_{k=1}^{N_h} \phi(x_k)\chi_{Q_k}(x), \tag{11}$$

where Q_j are disjoint subsets such that $\text{diam}(Q_j) \leq h$, $\bigcup_{j=1}^{N_h} Q_j = \Omega$, $x_j \in Q_j$, χ_E is the characteristic function of the set E, and ϕ is a suitable interpolant.

Consider the new system of equations as follows:

$$\frac{\partial \boldsymbol{u}}{\partial t} - \frac{Pr}{\sqrt{Ra}}\nabla^2\boldsymbol{u} + (\boldsymbol{u}\cdot\nabla)\boldsymbol{u} + \nabla p = Pr\Theta\boldsymbol{e}_2 - \mu_u(I_h(\boldsymbol{u}^o) - I_h(\boldsymbol{u})), \tag{12}$$

$$\frac{\partial \Theta}{\partial t} - \frac{1}{\sqrt{Ra}}\nabla^2\Theta + (\boldsymbol{u}\cdot\nabla)\Theta - \boldsymbol{u}\cdot\boldsymbol{e}_2 = -\mu_\theta(I_h(\Theta^o) - I_h(\Theta)), \tag{13}$$

$$\nabla\cdot\boldsymbol{u} = 0, \tag{14}$$

with initial conditions:

$$\boldsymbol{u}(0;(x,y)) = 0, \tag{15}$$

$$\Theta(0;(x,y)) = 0. \tag{16}$$

Let us denote the estimated solution of (12)–(16) as $V(t) = (\boldsymbol{u}(t), \Theta(t))$. To accurately predict $U(t)$ on the interval $[t_1,\ t_1+T]$, it is sufficient to have coarse observational data $I_h(U^o(t))$ accumulated over an interval of time $[0,\ t_1]$ linearly proportional to T in the immediate past [22].

In particular, suppose it is desired to predict $U(t)$ with accuracy $\epsilon > 0$ on the interval $[t_1,\ t_1+T]$, where t_1 is the present time and $T > 0$ determines how far into the future one wants to predict. Let h be small enough and μ_u be large enough, then there exist constants C and β such that

$$\|U(t) - V(t)\|_{H_1(\Omega)} \le Ce^{-\beta t},\ t \ge 0. \tag{17}$$

One then uses $V(t_1)$ as the initial condition to make future predictions. Let W be a solution of (1)–(5) with initial condition $W(t_1) = V(t_1)$. Known results on continuous dependence on initial conditions imply the existence of $\gamma > 0$ such that

$$\|W(t)-U(t)\|_{L_2(\Omega)} \le \|W(t_1)-U(t_1)\|_{L_2(\Omega)} e^{\gamma(t-t_1)},\ t \ge t_1. \tag{18}$$

Therefore,

$$\|W(t) - U(t)\|_{L_2(\Omega)} \le Ce^{-\beta t_1+\gamma T},\ t \in [t_1,\ t_1+T], \tag{19}$$

provided $\beta t_1 \ge \gamma T + \ln(C/\epsilon)$. Thus, $W(t)$ predicts $U(t)$ with accuracy ϵ on the interval $[t_1, t_1+T]$.

The traditional nudging algorithm as described above uses a combination of delta "functions" as a feedback term which may have serious issues at the PDE level. In the CDA algorithm, we implement an interpolant operator, I_h, and not a collection of delta "functions." At the level of numerical/computational implementation of the CDA PDE, one can discretize this PDE using a favorite numerical scheme and discretization (spectral, finite-elements, finite-differences, etc.) regardless of the nature of the mesh at which the observed data has been collected. The only natural condition should be, and is, that the mesh size of the downscaling numerical scheme for computing the algorithmic PDE should be finer than the size of the mesh of the collected data. In particular, there is no relationship between the computational mesh and the mesh on which the measurements are collected.

4 Numerical experiments

We implemented the 2D Bénard convection model in Matlab, as described in Section 2. We consider the box domain $[0, 2] \times [0, 1]$ uniformly discretized into 200×100 computational cells. The time step in our simulations is equal to 0.01 and a total of 3000 integration steps are performed. Our goal is to reconstruct, as accurately as possible, the solution $(\boldsymbol{u}(t);\ \Theta(t))$ of the Bénard convection problem on a

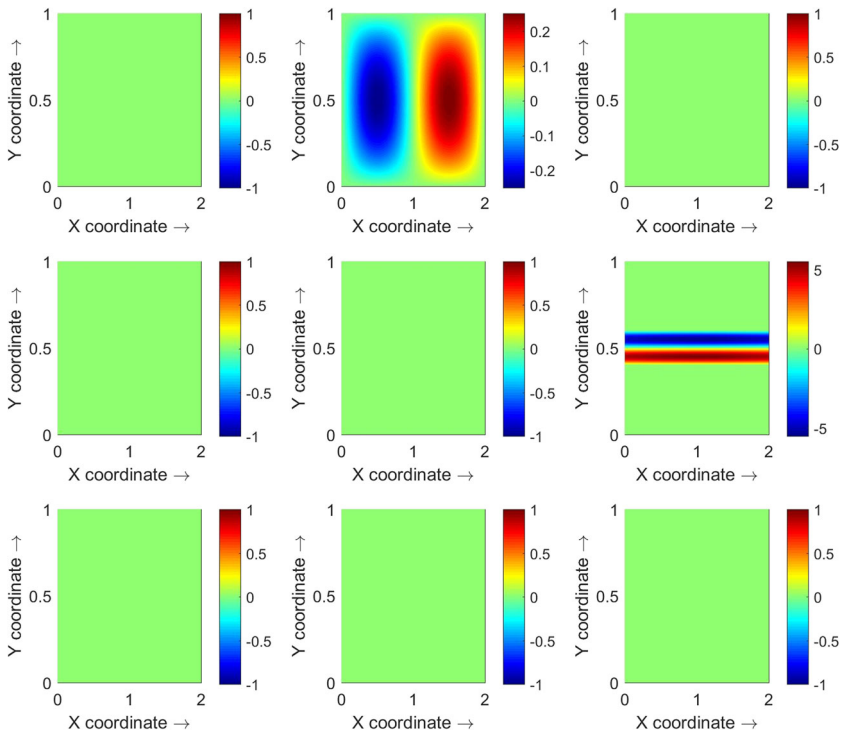

Fig. 1 Initial conditions for the background solution (*left panel*), reference solution (*middle panel*), and initial shear flow (*right panel*). *Top*: temperature, *middle*: u-velocity, and *bottom*: v-velocity

Table 1 Relaxation and nudging parameters for CDA and NA, respectively

Interpolant	Relaxation parameter (CDA)	Nudging parameter (NA)
Large	$\mu_\theta = 1.0, \mu_u = 1.0$	$\alpha_\theta = 3.5, \alpha_u = 3.5$
Medium	$\mu_\theta = 0.50, \mu_u = 0.50$	$\alpha_\theta = 2.5, \alpha_u = 2.5$
Small	$\mu_\theta = 0.10, \mu_u = 0.10$	$\alpha_\theta = 1.5, \alpha_u = 1.5$

high-resolution grid, using observations available on a much coarser grid using CDA. The results obtained using CDA are then compared with predictions of standard NA. We study the sensitivity of CDA to different choices of the interpolation operator I_h, and investigate the CDA robustness to observational noise and the spatial distribution of observations. We also provide an example in which temperature data alone are not enough to estimate the state of the Bénard equations (i.e., both temperature and velocities).

A reference model run was conducted with the initial conditions for temperature set as $\sin(\pi x)[y(y-1)]$, and the velocity initialized from rest (see Fig. 1) over the defined computational grid (i.e., 200×100 computational cells). The (downscaled) observations are extracted from the outputs of this reference run. The comparison of the two schemes (CDA and NA) is evaluated in terms of relative root mean square errors (RRMSE), computed as the ratio between the L_2-norm of the difference between the reference and downscaled solutions and the L_2-norm of the reference solution after every assimilation step. The experiments are performed with perfect and noisy observations to assess the robustness of both schemes to observational errors.

4.1 Sensitivity with respect to data grid resolution

Table 1 outlines the three values of relaxation parameters (μ_θ and μ_u) and nudging operators (α_θ and α_u) tested in the assimilation experiments with CDA and NA, respectively,

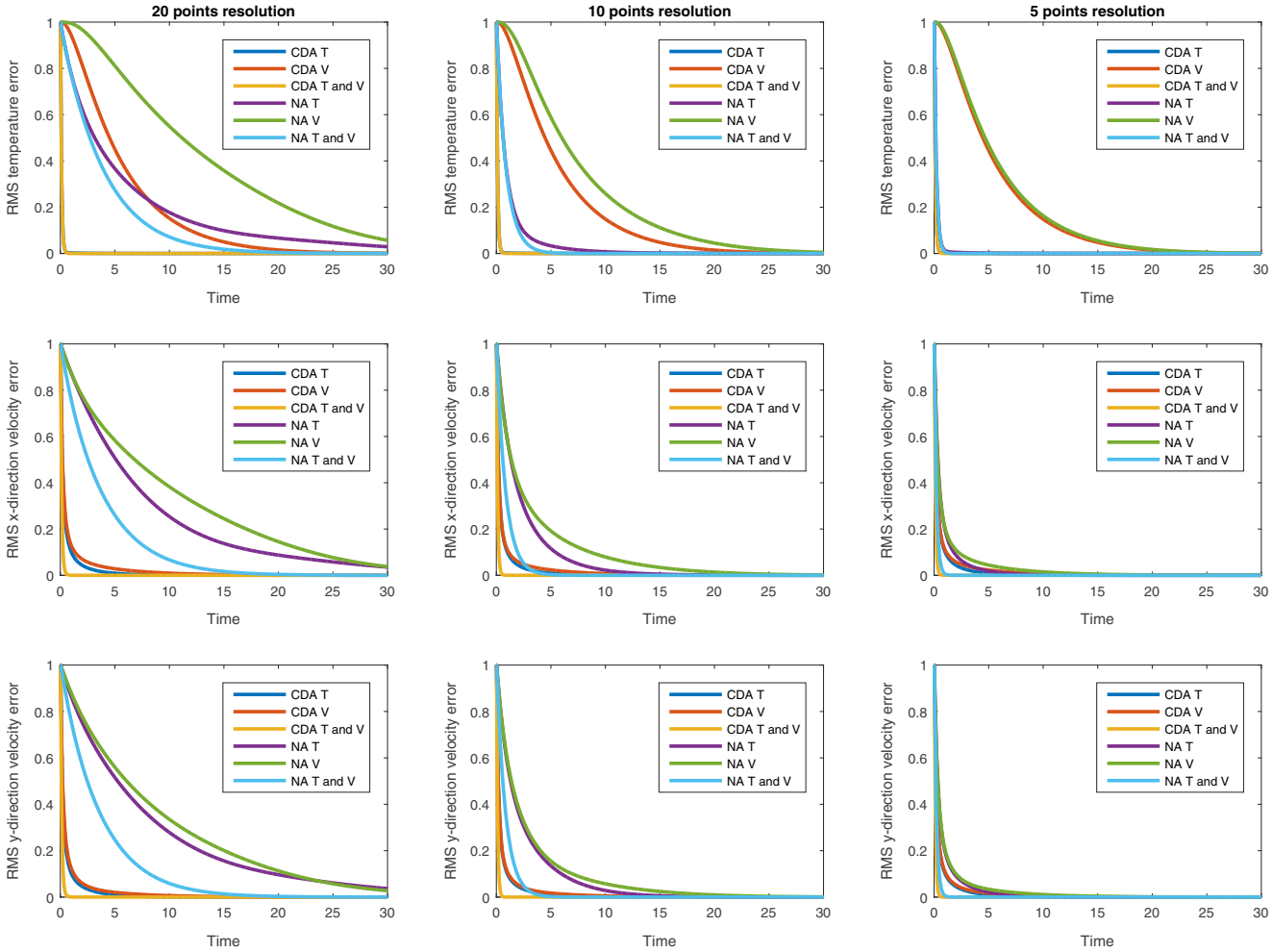

Fig. 2 CDA vs NA RRMSE results (CDA—$\mu_\theta = 0.10, \mu_V = 0.10$, NA—$\alpha_\theta = 1.50, \alpha_V = 1.50$). The *left panel* shows 20-point resolution, the *middle panel* shows 10-point resolution, and 5-point resolution on the *right panel*. The *blue curve* (CDA T) is overlapped by the *red line* (CDA T and V)

referred to as large, medium, and small. We conducted three experiments assimilating (i) velocity, (ii) temperature, and (iii) both velocity and temperature. Three observational scenarios are studied as follows: 1 out of 20 grid points in each direction of the high-resolution grid is assumed observed, for a total of 10×5 observed points; 1 out of 10 grid points in each direction, for a total of 20×10 observed points; and 1 out of 5 grid points in each direction, for a total of 40×20 observed points. Data were assimilated at every time step. We started the simulation from zero initial conditions for both temperature and velocity.

Figures 2, 3 and 4 plot the time evolution of the RRMSE with respect to the norm of the reference solution as they result from CDA and NA assimilating temperature, velocities, and both temperature and velocities. The results from three different scenarios and using different nudging coefficients suggest that CDA performs very well, showing significant improvements over NA estimates. The convergence of CDA is clearly faster than NA as depicted in Fig. 2. When assimilating either temperature (i.e., $\mu_u = 0$) or both velocity and temperature, an exponential convergence is obtained for both velocity and temperature for all the three choices of grid resolution. This is not true for NA, which achieves an exponential convergence only for the case when a dense observation network is used (i.e., 1 out of 5 point grid resolution).

When assimilating only velocity (i.e., $\mu_\theta = 0$), both temperature and velocity converge, but velocity converges faster. In the case of velocity, the choice of relaxation parameter μ_u plays an important role as can be seen from Figs. 2, 3 and 4. Using larger values of μ_u, the velocity converges to the reference solution exponentially. This suggests that for the given set of initial conditions, velocity and temperature measurements alone are enough to determine all the fields in the 2D Bénard convection model using CDA as demonstrated in [27]. The results further demonstrate that CDA is robust and not very sensitive to the choice of relaxation parameters (μ_θ and μ_u). The snapshots of

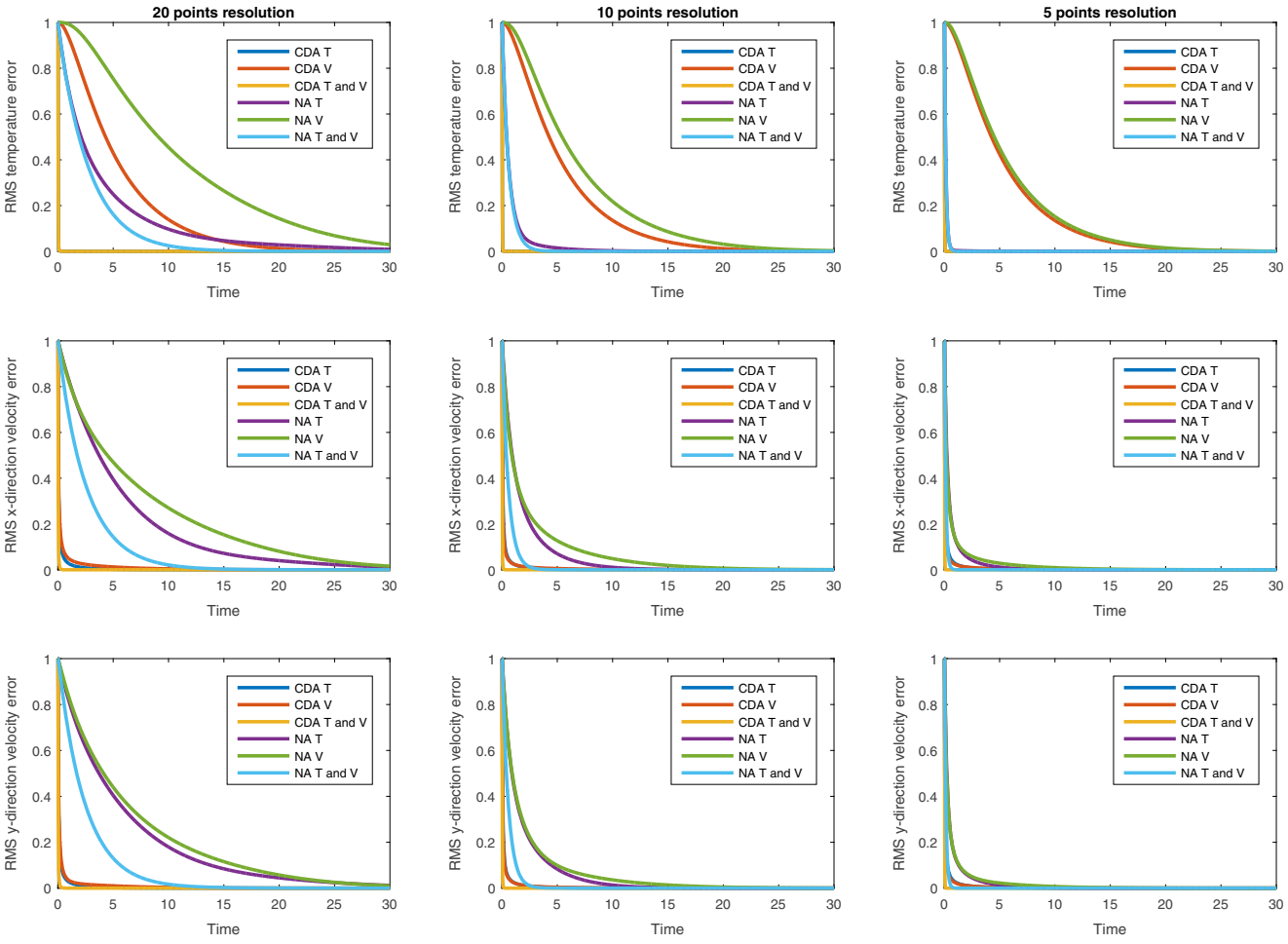

Fig. 3 CDA vs NA RRMSE results (CDA—$\mu_\theta = 0.50, \mu_V = 0.50$, NA—$\alpha_\theta = 2.50, \alpha_V = 2.50$). The *left panel* shows 20-point resolution, the *middle panel* shows 10-point resolution, and 5-point resolution on the *right panel*. The *blue curve* (CDA T) is overlapped by the *red line* (CDA T and V)

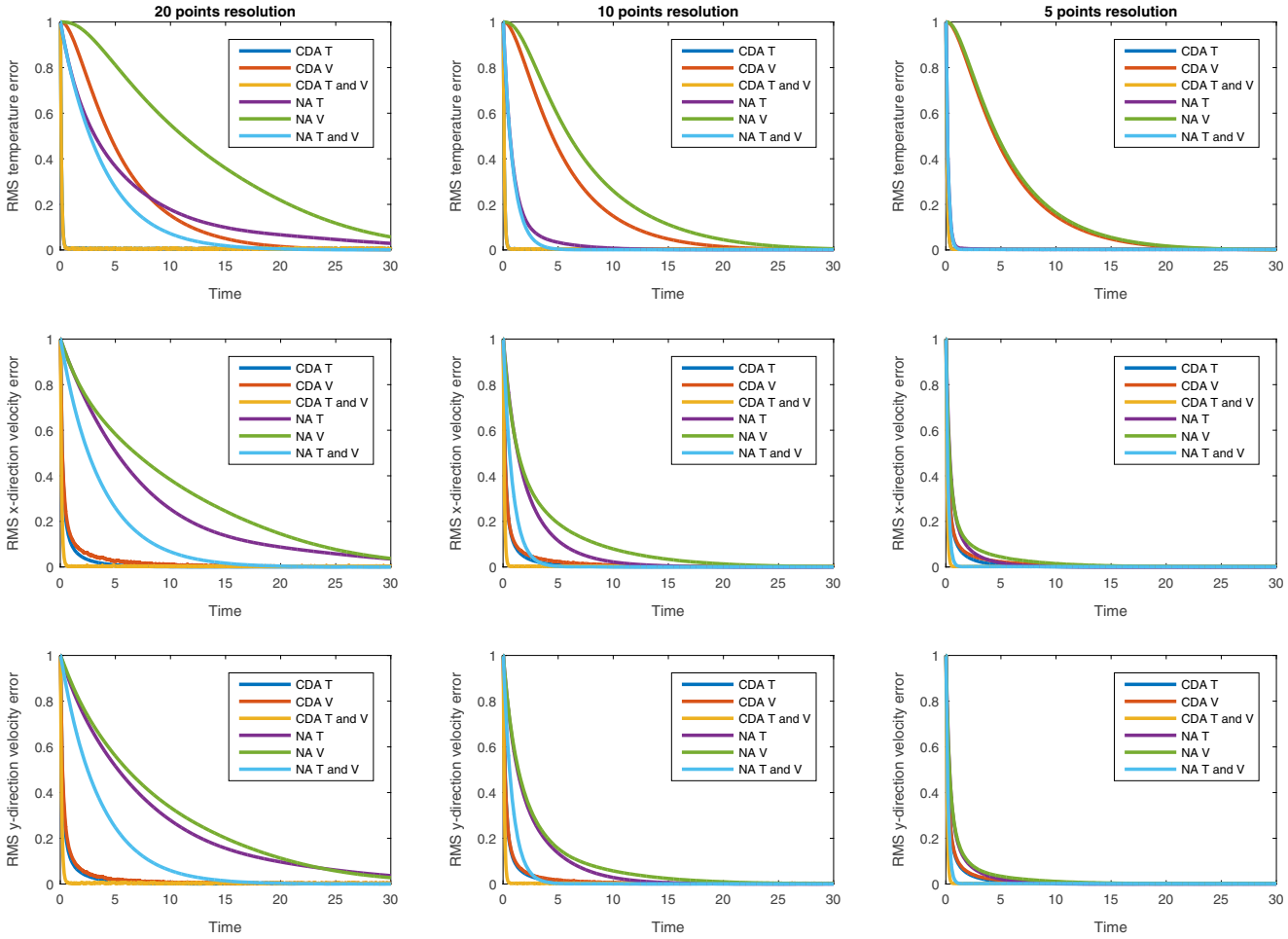

Fig. 4 CDA vs NA RRMSE results (CDA—$\mu_\theta = 1.0$, $\mu_V = 1.0$, NA—$\alpha_\theta = 3.50$, $\alpha_V = 3.50$). The *left panel* shows 20-point resolution, the *middle panel* shows 10-point resolution, and 5-point resolution on the *right panel*. The *blue curve* (CDA T) is overlapped by the *red line* (CDA T and V)

the assimilated temperature and velocity data at the end of assimilation window are presented in Figs. 5, 6, and 7. These figures show that both CDA and NA converge to the reference solutions at the end of the assimilation window.

4.2 Sensitivity with respect to time frequency of the data

We also investigated the sensitivity of CDA and NA to the frequency of available data in time. Here, we assume that the data are available every 10 and 20 time steps and assimilated both temperature and velocity. We implemented four different strategies as follows:

- NA-Time: NA with relaxation of the model solution only at the time when the observations are available every 10 and 20 time steps.
- CDA-Time: CDA with relaxation of the model solution only at the time when the observations are available every 10 and 20 time steps.

Figures 8 and 9 present the results of these experiments compared to the cases where observations are available at every time step. The left and right panels of Figs. 8 and 9 show the RRMSE with 1 out of 20-point and 1 out of 10-point grid resolutions, respectively. Even when the data are assimilated every 10 and 20 time steps, CDA and CDA-time converge exponentially in time, and there are no obvious differences in their RRMSEs. In contrast, the results of NA and NA-time significantly differ in terms of time and grid nudging. This indicates that CDA is much more robust than NA in the case when the observations are coarse in time, and that it achieves fast convergence for both velocity and temperature.

4.3 Sensitivity of CDA to the interpolation operator

We also study the sensitivity of CDA to the choice of the interpolation operator, examining the impact of smoother interpolants. To do that, we set up an experiment in

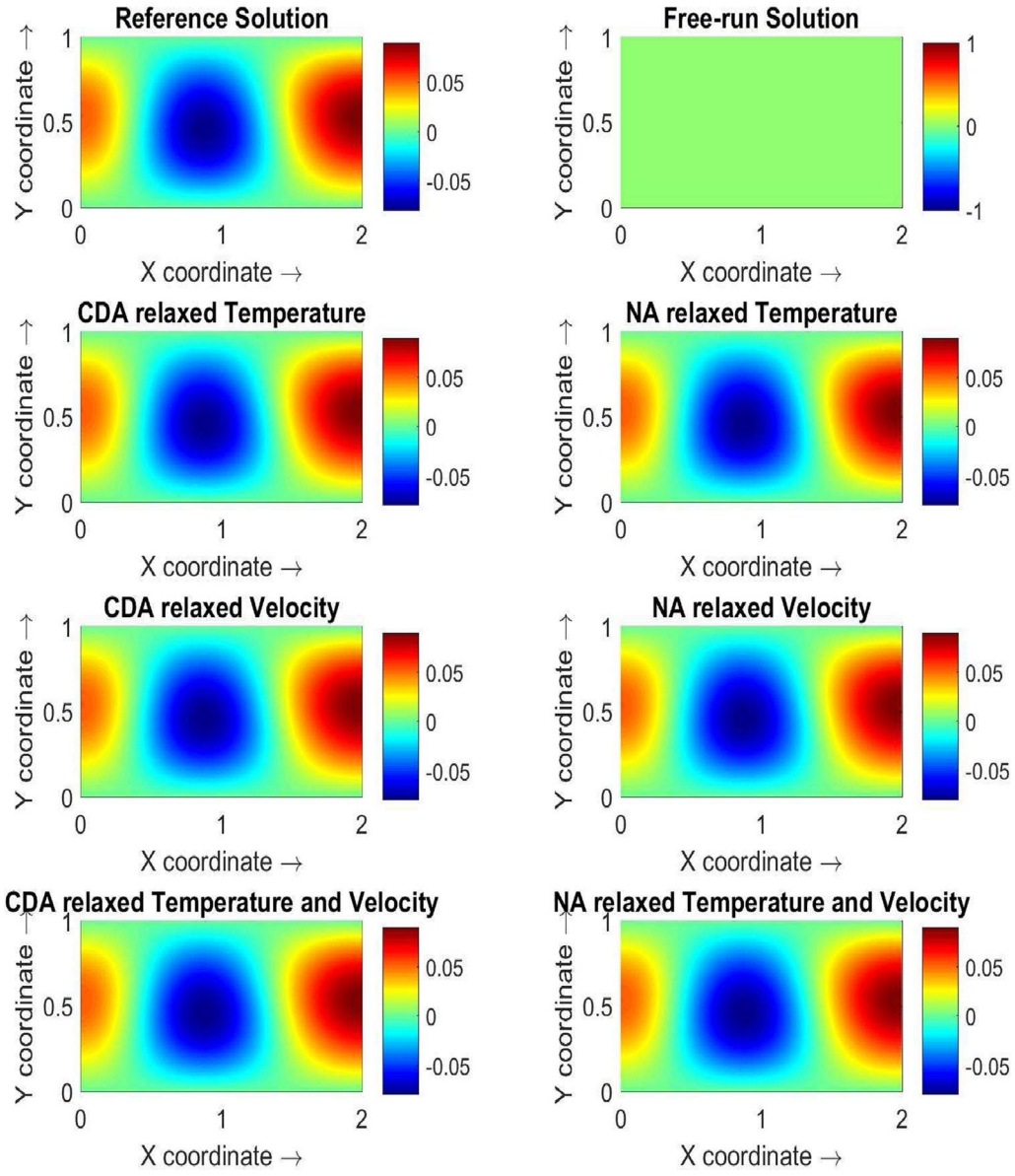

Fig. 5 Temperature field at time ($t = 30$) and assimilation of data every 10-point grid resolution as it results from CDA and NA with assimilation of different variables (CDA—$\mu_\theta = 0.10, \mu_V = 0.10$, NA—$\alpha_\theta = 1.50, \alpha_V = 1.50$). The simulation starts from rest (Fig. 1—*left panel*). The free-run solution is the result of simulation with zero initial conditions without data assimilation

which the data are available using 10 time steps and every 1 out of 10 grid points. Four different interpolation operators are tested (see Table 2 for details). The RRMSE results presented in Fig. 10 suggest that the CDA method is equally efficient for all the interpolation operators.

In terms of computational cost, we examined the CDA method with respect to each interpolation operator. For this, we have assumed that the data is available every 10^{th} grid point for (1) each time step and (2) every 10^{th} time step and assimilated both temperature and velocity. The costs of these runs are then compared to those of NA. Figure 11 plots the CPU usage of CDA interpolation schemes vs NA. It is evident that CDA converges exponentially, and there is no significant difference in terms of computational costs of CDA with the different interpolation schemes compared to NA, especially when data are assimilated every 10 time steps.

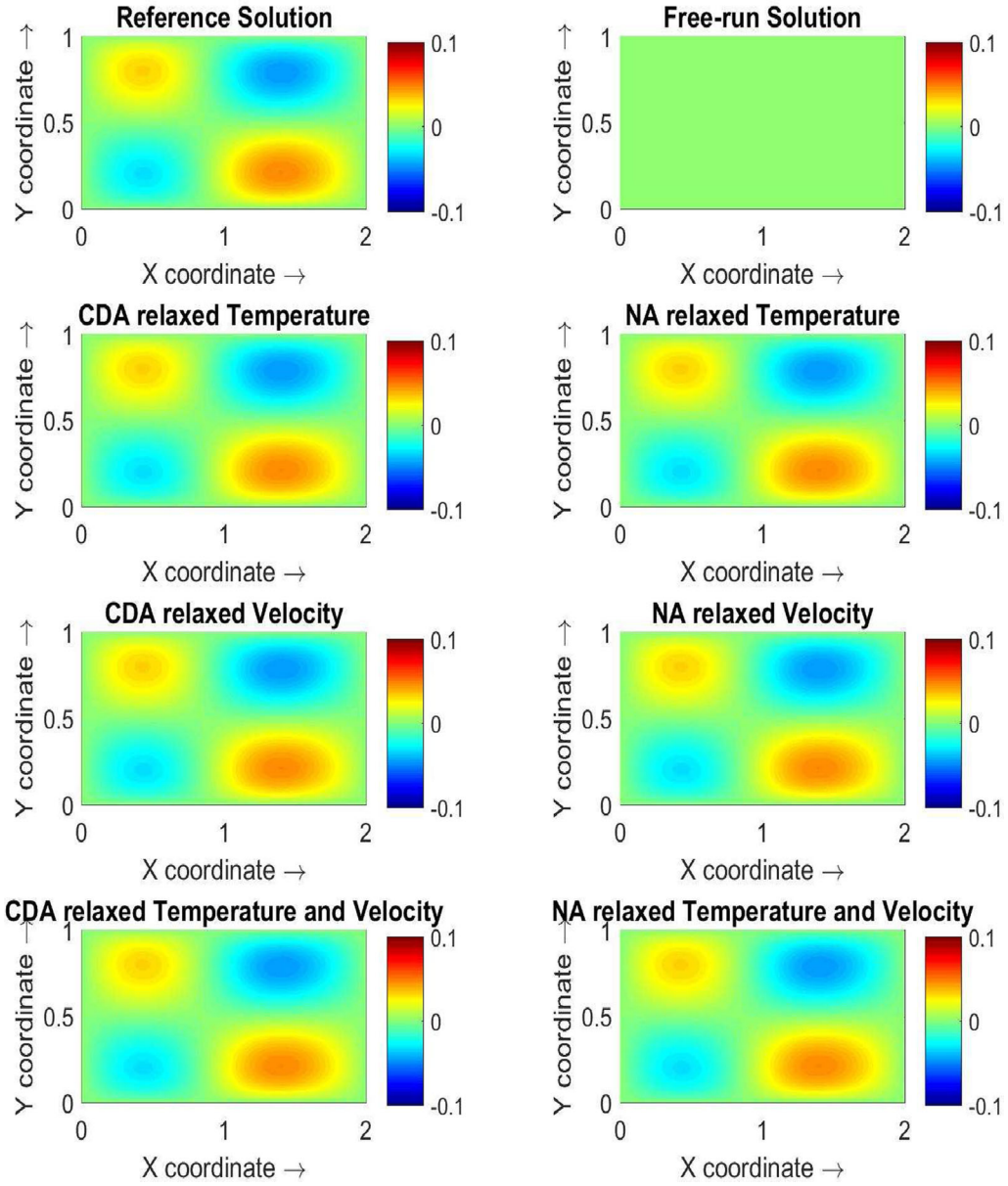

Fig. 6 x-direction of velocity field at time ($t = 30$) and assimilation of data every 10-point grid resolution as it results from CDA and NA with assimilation of different variables (CDA—$\mu_\theta = 0.10$, $\mu_V = 0.10$, NA—$\alpha_\theta = 1.50$, $\alpha_V = 1.50$). The simulation starts from rest, i.e., $u = 0$ (Fig. 1—*left panel*). The free-run solution is the result of simulation with zero initial conditions without data assimilation

4.4 Sensitivity to observational errors

The above experiments assimilated perfect observations, meaning that they were exactly the values as extracted from the reference model run. In practical applications, however, observations are collected by measurements and those are prone to noise. Therefore, it is important to investigate the sensitivity of CDA to data noise.

To simulate the situation of noisy observations, perturbations were induced in the process of obtaining the reference solution. Each entry in the observations set was multiplied by a random number (uniformly distributed) between $1 + \varepsilon$ and $1 - \varepsilon$, corresponding to measuring with a relative error of ε. The experiments were performed with ε values of 0.05. We have used two values of relaxation parameters (μ_θ and μ_u) and nudging operators (α_θ and α_u), referred to as large

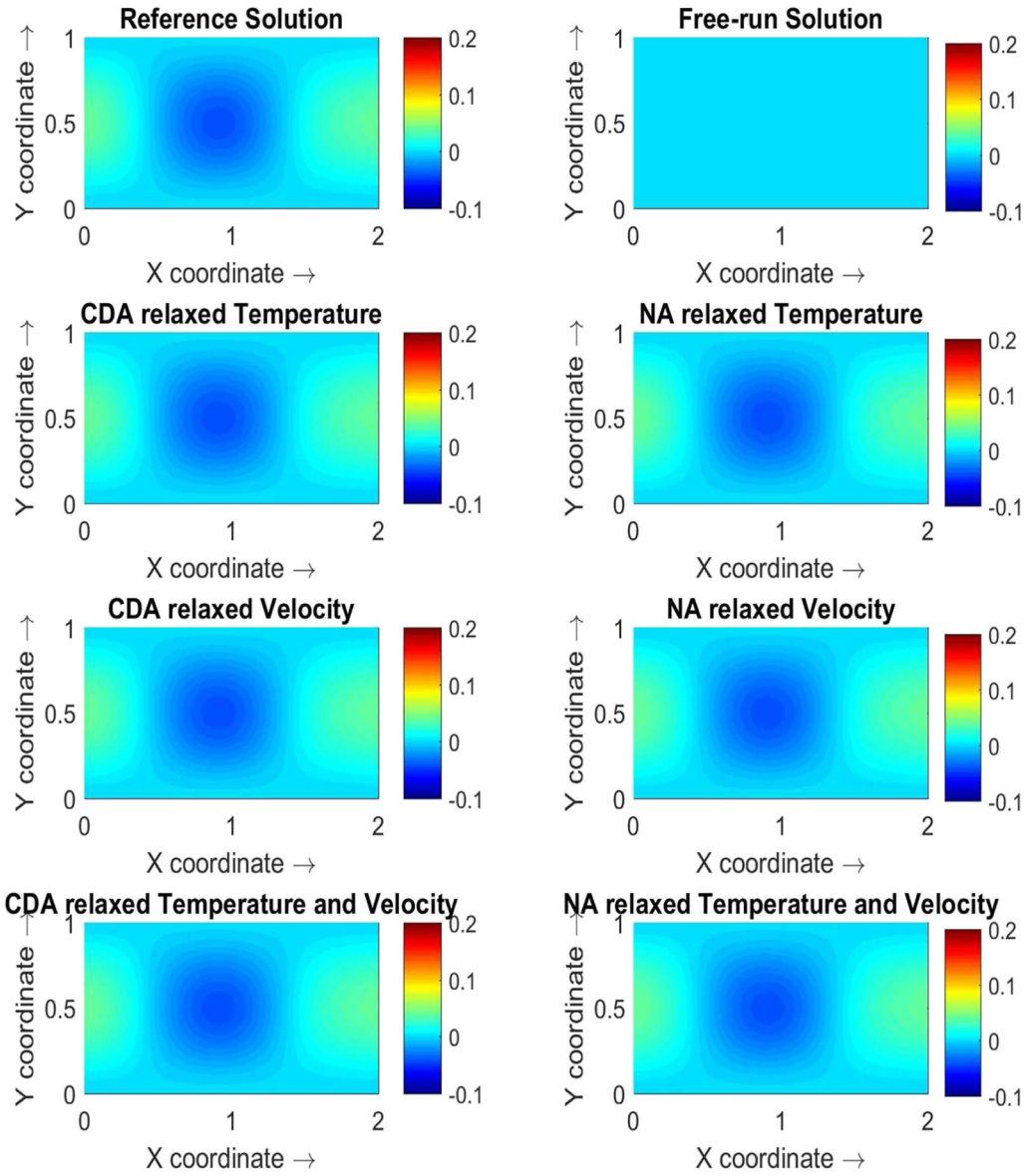

Fig. 7 y-direction of velocity field at the end of the assimilation window ($t = 30$) and assimilation of data every 10-point grid resolution as it results from CDA and NA with assimilation of different variables (CDA—$\mu_\theta = 0.10, \mu_V = 0.10$, NA—$\alpha_\theta = 1.50, \alpha_V = 1.50$). The simulation starts from rest, i.e., $v = 0$ (Fig. 1—*left panel*). The free-run solution is the result of simulation with zero initial conditions without data assimilation

and small in Table 1. The data are assimilated every time step using the 20-, 10-, and 5-grid point resolution. The results are presented in Figs. 12 and 13. The RRMSE results are not impacted by the observational noise for small relaxation parameters ($\mu_\theta = 0.10$ and $\mu_u = 0.10$), in contrast to the CDA runs with large values of relaxation parameters ($\mu_\theta = 1.0$ and $\mu_u = 1.0$) which reveal a slight impact on the RRMSE values, especially for the case of coarse data assimilating temperature and velocity every 20^{th} grind point. This is expected since larger values of relaxation parameters more strongly nudge the model toward the perturbed observations. Also note that although NA exhibits a slow convergence rate, its results are also sensitive to noise in the observations.

4.5 Assimilation using temperature only: a counter example

For the present setting, the possibility of assimilating all field variables based on observations of the velocity

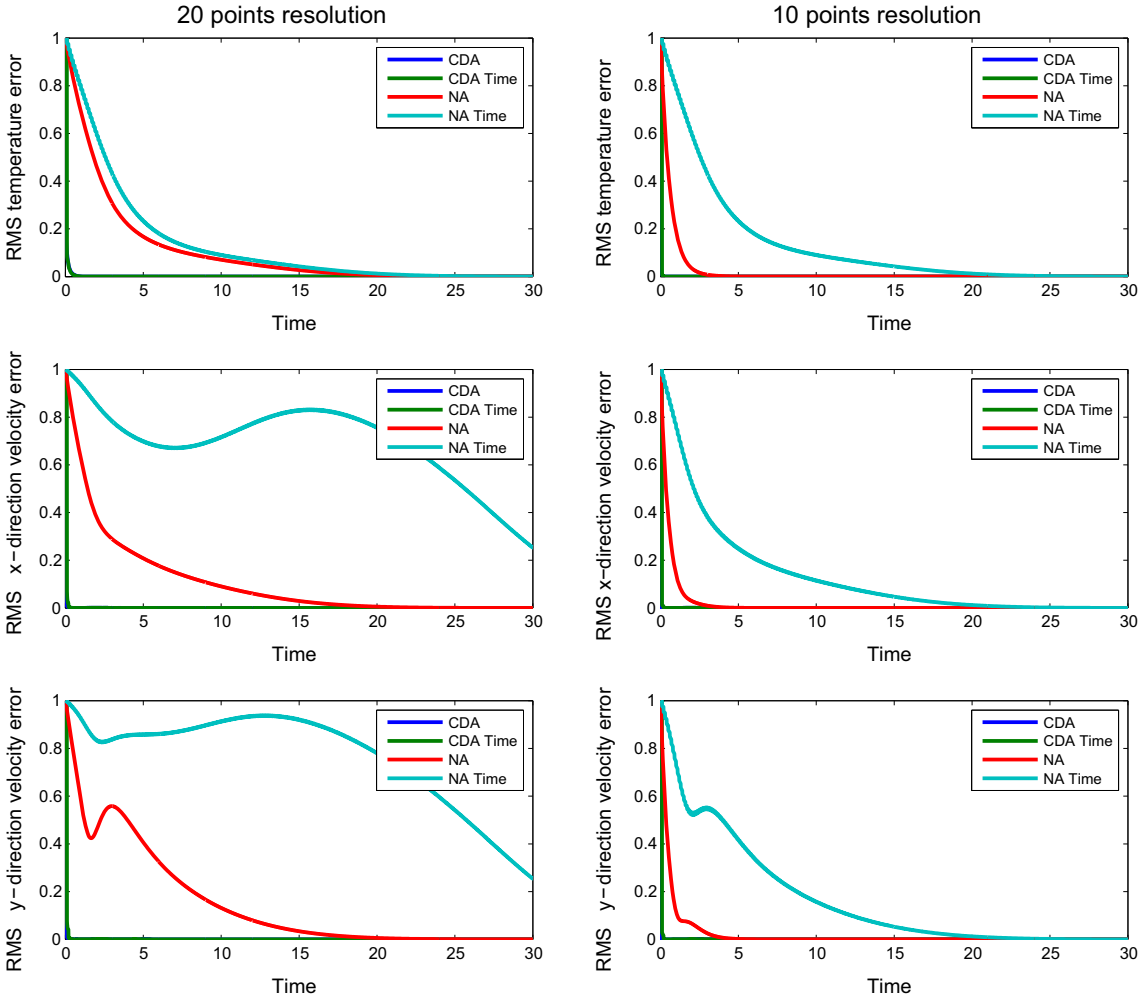

Fig. 8 Sensitivity of CDA and NA to the availability of data every 10^{th} time steps (CDA—$\mu_\theta = 0.50$, $\mu_V = 0.50$, NA—$\alpha_\theta = 2.50$, $\alpha_V = 2.50$). The simulation starts from zero initial conditions (Fig. 1—*left panel*). The *blue curve* (CDA) is overlapped by the *green line* (CDA Time)

alone was established rigorously. The numerical experiments above exhibited results that are consistent with the theory. The simulations also showed that in many cases, coarse temperature observations can be sufficient for predicting both the temperature and velocity fields. However, we do not expect coarse temperature observations to be sufficient in general. Intuitively, two scenarios immediately come to mind that signal potential deficiencies. One concern is the situation where the Prandtl number is small. In this case, temperature gradients tend to equilibrate at a much higher rate than regions of high shear, leading to insufficient information about the structure of the velocity field. Another situation concerns the existence of purely horizontal shear, which can exist in the absence of a temperature gradient.

In this section, we conduct a numerical experiment, inspired by the latter observation, demonstrating that assimilation of only temperature measurements may not lead to the recovery of the true state. In the present experiment, the initial condition for the x-direction velocity is as follows:

$$u(x, y, 0) = \begin{cases} 5\sin(10\pi y)[1 + 0.1\sin(\pi x)], & \text{for } 0.4 \le y \le 0.6, \\ 0, & \text{otherwise,} \end{cases}$$

representing a strong velocity shear in the center of the domain. A mode 1 perturbation is imposed in order to trigger the development of the Kelvin-Helmholtz (KH) instability. The initial temperature field is set to zero (see Fig. 1,

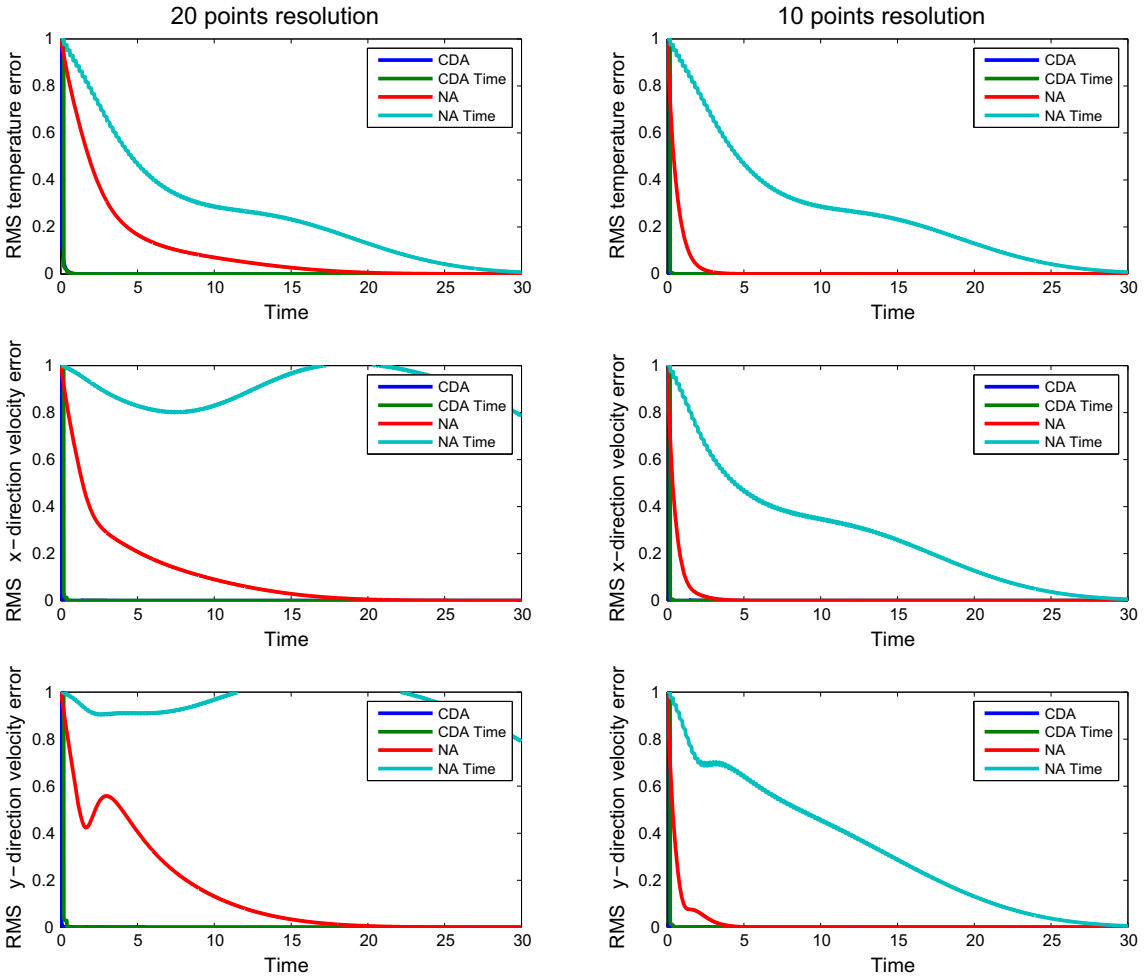

Fig. 9 Sensitivity of CDA and NA to the availability of data every 20^{th} time steps (CDA—$\mu_\theta = 0.50$, $\mu_V = 0.50$, NA—$\alpha_\theta = 2.50$, $\alpha_V = 2.50$). The simulation starts from zero initial conditions (Fig. 1—*left panel*). The *blue curve* (CDA) is overlapped by the *green line* (CDA Time)

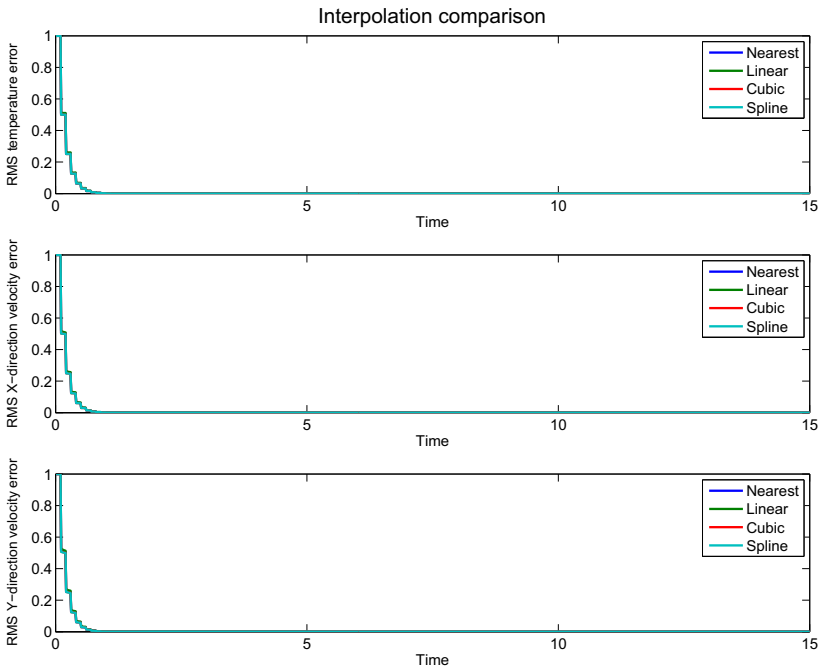

Fig. 10 Sensitivity of CDA to the choice of the interpolation operator with 10-point grid resolution every 10^{th} time step (CDA—$\mu_\theta = 0.50$, $\mu_V = 0.50$, NA—$\alpha_\theta = 2.50$, $\alpha_V = 2.50$). The simulation starts from zero initial conditions (Fig. 2—*left panel*). All curves overlap and show similar convergence for all the interpolation operators

Table 2 2D interpolation operators

Interpolant	Details
Nearest	Discontinuous
Linear	$C([0,1]\times[0,1])$
Cubic	$C^1([0,1]\times[0,1])$
Spline	$C^2([0,1]\times[0,1])$

right panel). We performed an experiment assimilating (i) velocity, namely using $\mu_u = 1$ and $\mu_\theta = 0$; (ii) temperature, namely using $\mu_u = 0$ and $\mu_\theta = 10$; and (iii) both velocity and temperature, namely with $\mu_u = 1$ and $\mu_\theta = 10$. The experiment relied on a 4-point grid resolution, with a time step $\Delta t = 0.001$. The rest of the experimental setup is the same as in Section 4.1.

Figure 14 compares curves of RRMSE with respect to the norm of the reference solution as they result from CDA assimilating different types of data. The following conclusions can be drawn from this experiment:

– When assimilating only temperature with CDA (i.e., $\mu_u = 0$), the temperature converges exponentially, but the velocity starts to converge only when the shear is dissipated.
– When assimilating velocity (i.e., $\mu_\theta = 0$) or both temperature and velocity with CDA, both temperature and velocity converge exponentially.

Instantaneous distributions of the assimilated temperature and velocity components are presented in Figs. 15, 16, and 17, based on results obtained with $\mu_u = 1$ and $\mu_\theta = 10$. The figures show that in the initial stages of the simulation, concentrated vortices appear due to the evolution of the KH instability. The growth of the instability saturates quickly (around $t = 5$), and the strength of the eddies starts to diminish due to the action of viscous forces. As the KH eddies start to decay, the Rayleigh-Bénard instability starts to amplify, eventually leading to a similar flow pattern as observed when a quiescent flow initial condition is used. The observed behavior thus indicates that for the present case, the flow is shear dominated in the initial stages of the simulation, whereas it is buoyancy-dominated at later stages. This illustrates the fact that in the presence of strong shear, assimilation of temperature data alone may not recover the true solution. This is consistent with the results in Fig. 14, which show for $\mu_u = 0$ the RRMSE curve is essentially flat for an extended time period following the start of the simulation.

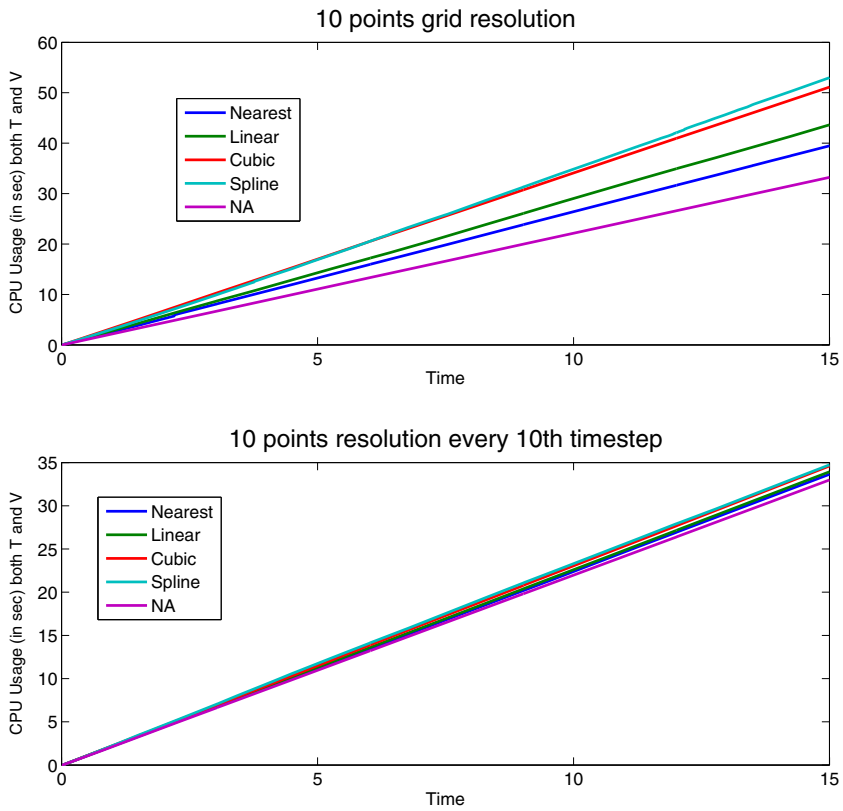

Fig. 11 Efficiency of CDA vs NA for 10-point grid resolution (CDA—$\mu_\theta = 0.50$, $\mu_V = 0.50$, NA—$\alpha_\theta = 2.50$, $\alpha_V = 2.50$). The simulation starts from zero initial conditions (Fig. 1—*left panel*)

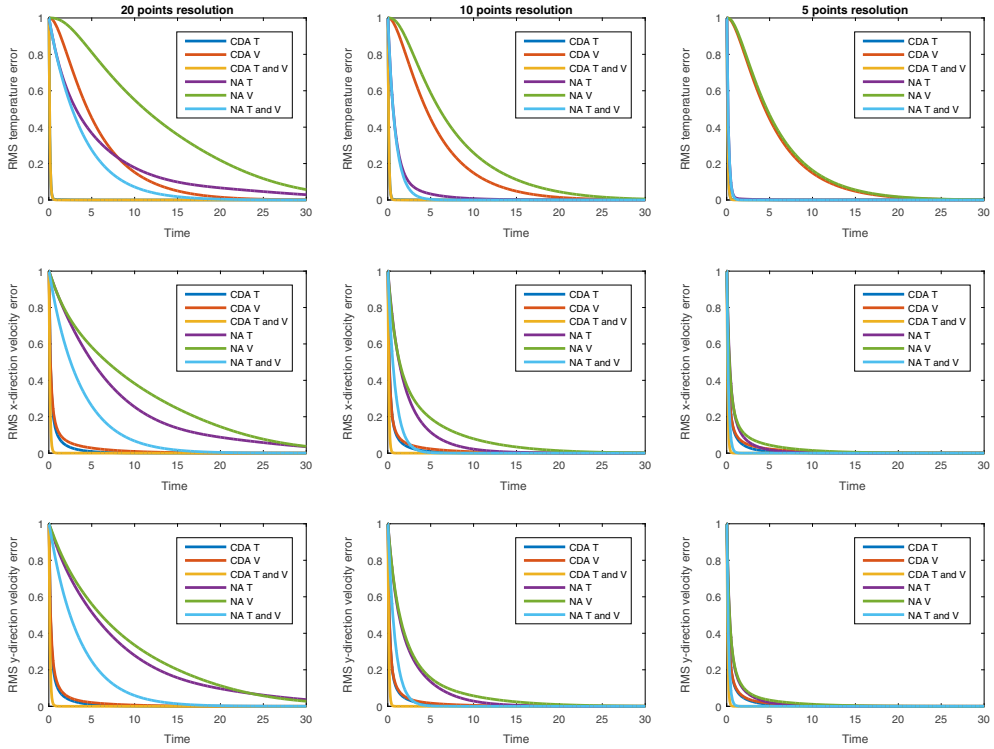

Fig. 12 CDA vs NA RRMSE results with perturbed data (5%) (CDA—$\mu_\theta = 0.1, \mu_V = 0.1$, NA—$\alpha_\theta = 1.50, \alpha_V = 1.50$). The left panel shows 20-point resolution, the *middle panel* shows 10-point resolution, and 5-point resolution on the *right panel*. The simulation starts from zero initial conditions (Fig. 1—*left panel*). The *blue curve* (CDA T) is overlapped by the red line (CDA T and V)

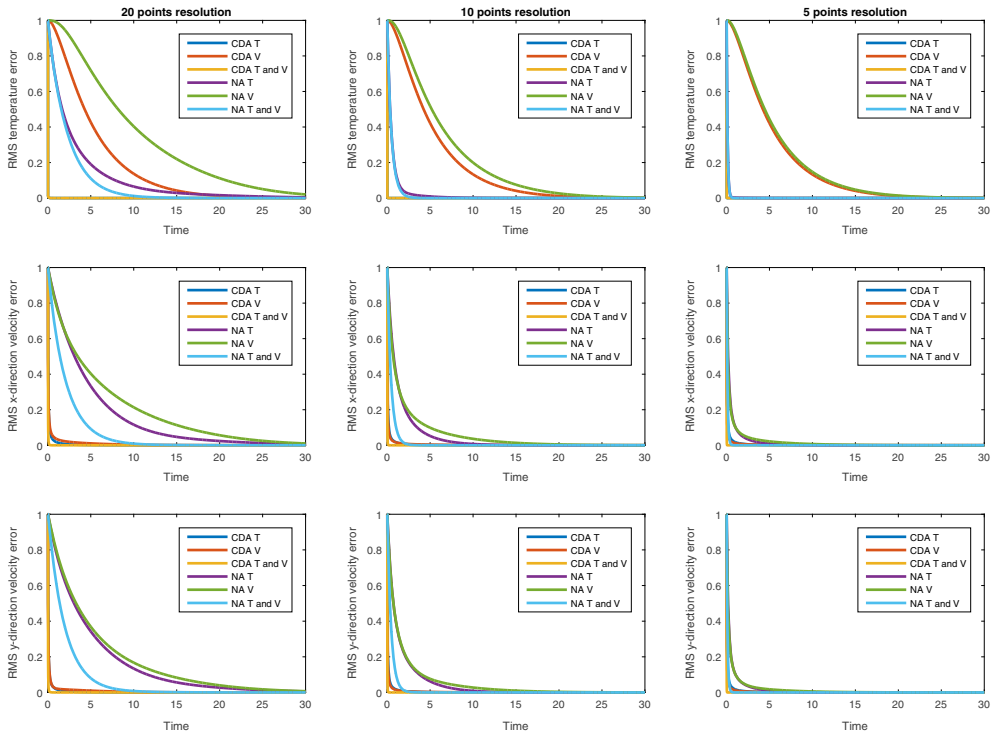

Fig. 13 CDA vs NA RRMSE results with perturbed data (5%) (CDA—$\mu_\theta = 1.0, \mu_V = 1.0$, NA—$\alpha_\theta = 3.50, \alpha_V = 3.50$). The *left panel* shows 20-point resolution, the *middle panel* shows 10-point resolution, and 5-point resolution on the *right panel*. The simulation starts from zero initial conditions (Fig. 1—left panel). The *blue curve* (CDA T) is overlapped by the *red line* (CDA T and V)

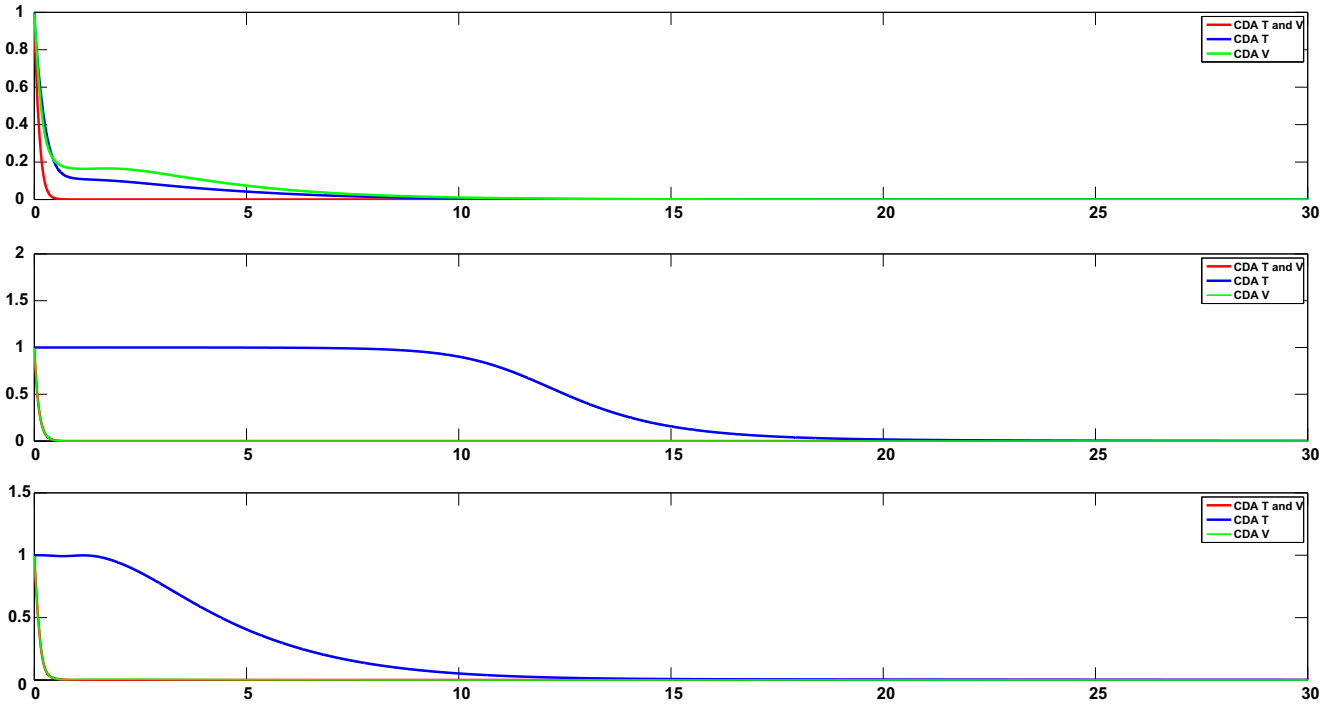

Fig. 14 CDA RRMSE results (CDA—$\mu_\theta = 10$, $\mu_V = 10$) with new set of initial condition and 4-point resolution

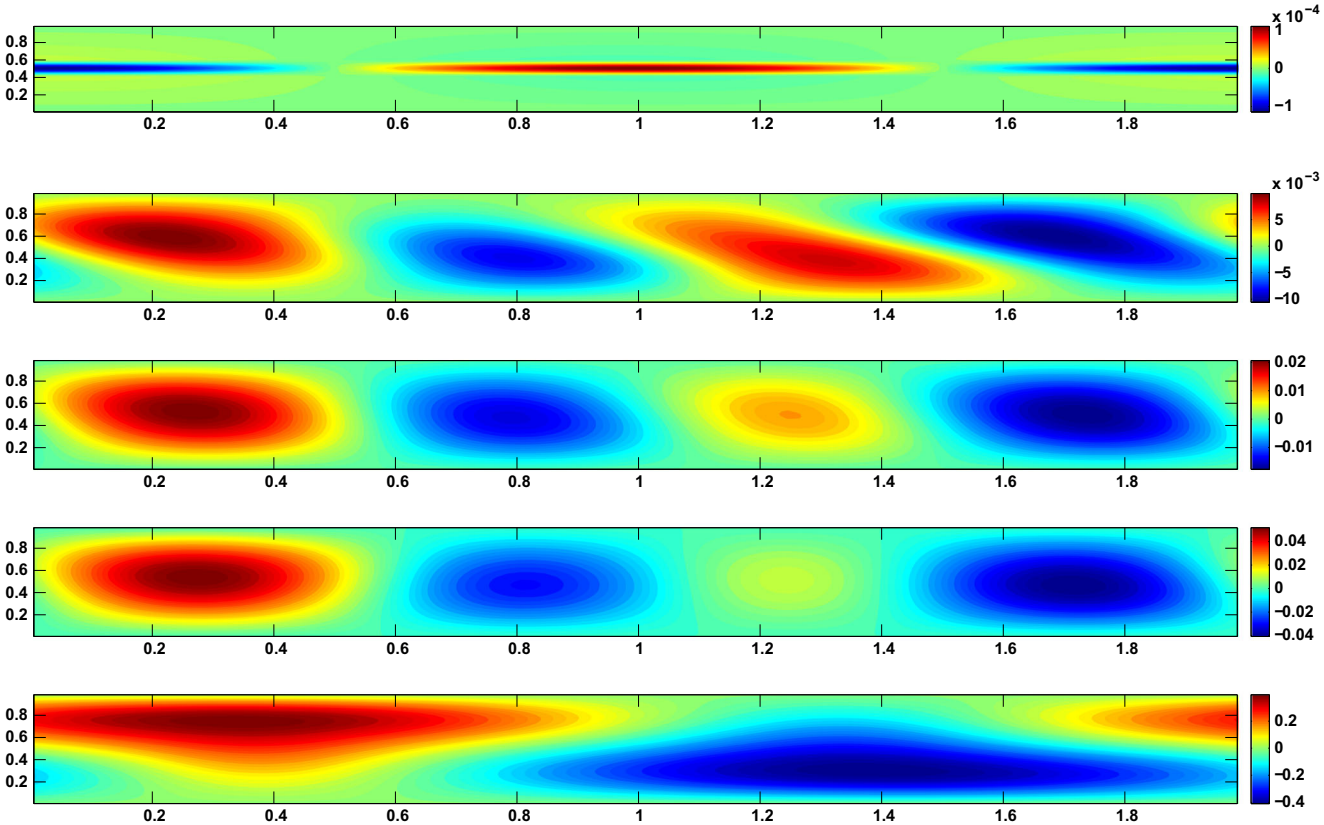

Fig. 15 Temperature field at the assimilation windows $t = 0, 5, 10, 15,$ and 30 (*top to bottom*). The data is assimilated every 4-point grid resolution as it results from CDA with relaxation parameters ($\mu_\theta = 10$, $\mu_V = 1.0$). The simulation starts from a perturbed shear flow (Fig. 1—*right panel*)

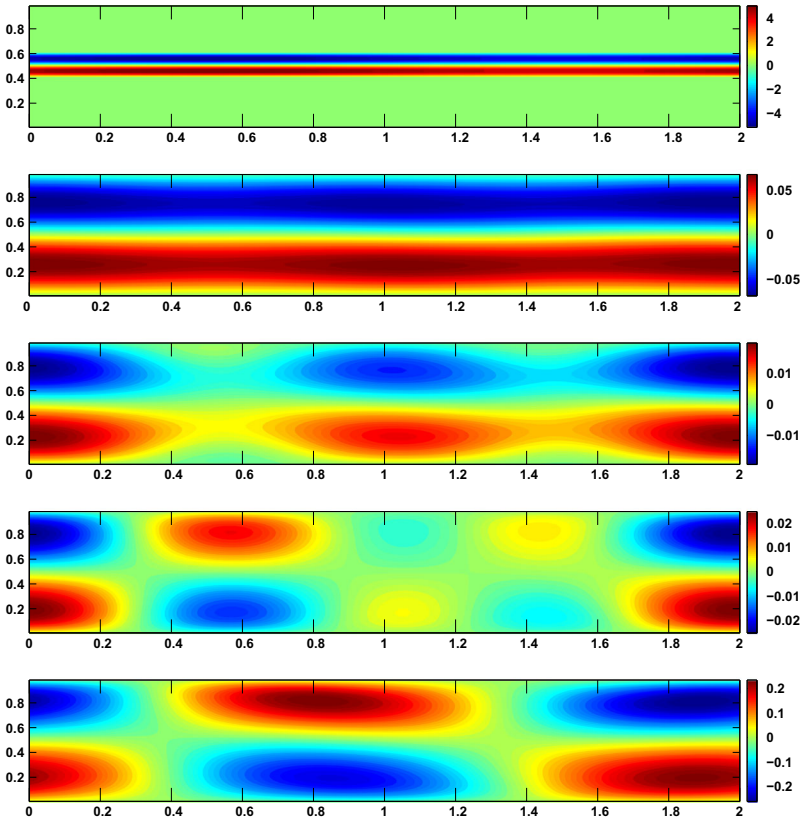

Fig. 16 x-direction of velocity field at the assimilation windows $t = 0, 5, 10, 15$, and 30 (*top to bottom*). The data is assimilated every 4-point grid resolution as it results from CDA with relaxation parameters ($\mu_\theta = 10, \mu_V = 1.0$). The simulation starts from a perturbed shear flow (Fig. 1—*right panel*)

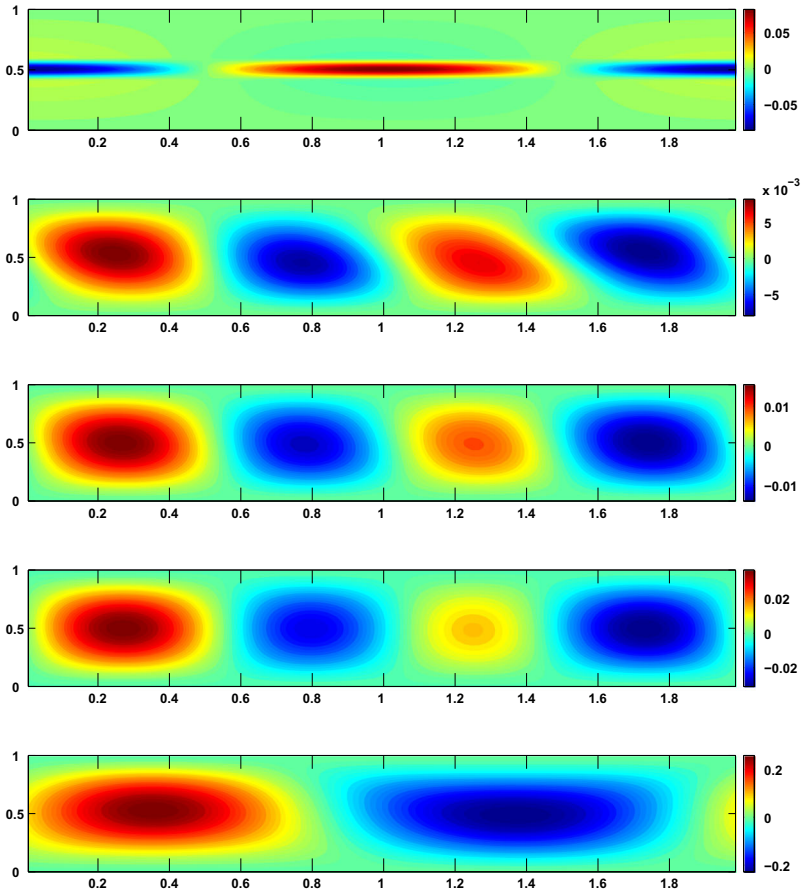

Fig. 17 y-direction of velocity field at the assimilation windows $t = 0, 5, 10, 15$, and 30 (*top to bottom*). The data is assimilated every 4-point grid resolution as it results from CDA with relaxation parameters ($\mu_\theta = 10, \mu_V = 1.0$). The simulation starts from a perturbed shear flow (Fig. 1—*right panel*)

5 Conclusions

Dynamical downscaling (DD) methods are needed to compute local-scale weather and climate from the outputs of global circulation models (GCMs). Nudging-based methods are often used for DD to force regional circulation model (RCM) simulations towards large-scale driving data. In this paper, the continuous data assimilation (CDA) algorithm is implemented and tested in the context of DD for the 2D Bénard convection model using coarse mesh measurements of the temperature and velocity.

Various numerical experiments are performed with CDA assimilating velocity, temperature, and both velocity and temperature. The results obtained from these experiments are compared with the standard point-to-point grid nudging method and demonstrate that CDA is more robust than NA and is not sensitive to the choice of control parameters. It is also shown that assimilating only velocity, both temperature and velocity converge, though velocity converges faster. On the other hand, assimilating only temperature does not necessarily recover the velocity field. This is demonstrated using an example where assimilation starts from an initial shear flow. In particular, the results indicate that in this case, the estimated velocity field suffers from large errors.

In addition, we have examined the sensitivity of CDA and grid nudging methods with respect to the level of noise in the assimilated observations and the spatial and temporal frequencies of observation points. In both cases, CDA was found to be more performant and robust than the standard grid nudging, although slightly sensitive to the choice of the relaxation parameter when observations are noisy. In this work, we have followed the common practice and the current CDA theoretical framework and assumed the observational errors to be uncorrelated, in space and time. While measurement errors could be always made uncorrelated in space via a judicious transformation of the data (with the inverse of the square-root of the observational error covariance), it is still not clear how to deal with time-correlated measurement errors, and their impact on CDA. This could be important in some situations when the data are collected with the same instrumentation, and will be considered in our future research.

Our overall results suggest that CDA is easy to implement and provides an efficient and robust approach for dynamical downscaling of the 2D Bénard convection model. It was further found more performant that the standard grid nudging at equivalent computational requirements. Our next step will be to test CDA for downscaling ocean and atmospheric global fields using general circulation models.

Acknowledgments The work of E.S.Titi was supported in part by the ONR grant N00014-15-1-2333 and the NSF grants DMS-1109640 and DMS-1109645.

References

1. Timbal, A., Dufour, A., McAvaney, B.: An estimate of future climate change for Western France using a statistical downscaling technique. Climate Dyn. **20**, 807–823 (2003)
2. Hewitson, B.C., Crane, R.G.: Consensus between GCM climate change projections with empirical downscaling: precipitation downscaling over South Africa. Int. J. Climatol. **26**, 1315–1337 (2006)
3. Gutzler, D.S., Robbins, T.O.: Climate variability and projected change in the western United States: regional downscaling and drought statistics. Clim. Dyn. **37**, 835–849 (2011)
4. Jha, S.K., Mariethoz, G., Evans, J., McCabe, M.F., Sharma, A.: A space and time scale-dependent nonlinear geostatistical approach for downscaling daily precipitation and temperature. Water Resour. Res. **51**(8), 6244–6261 (2015)
5. Guiterrez, J.M., San-Martin, D., Brands, S., Manzanas, R., Herrera, S.: Reassessing statistical downscaling techniques for their robust application under climate change conditions. J. Climate **26**, 171–188 (2013)
6. McGregor, J.: Regional climate modelling. Meteorol. Atmos. Phys. **63**, 105–117 (1997)
7. Liu, P., Tsimpidi, A.P., Hu, Y., Stone, B., Russell, A.G., Nenes, A.: Differences between downscaling with spectral and grid nudging using WRF. Atmos. Chem. Phys. **12**, 3601–3610 (2012)
8. Feser, F., Barcikowska, M.: The influence of spectral nudging on typhoon formation in regional climate models. Environ. Res. Lett. **7**(1), 014024 (2012)
9. Lo, C.J., Yang, Z.L., Pielke, R.A.: Assessment of three dynamical climate downscaling methods using the weather research and forecasting (WRF) model. J. Geophys. Res. **113**, D09112 (2012)
10. Wilby, R., Wigley, L.T.M.L.: Downscaling general circulation model output: a review of methods and limitations. Prog. Phys. Geog. **21**, 530—548 (1997)
11. Murphy, J.: An evaluation of statistical and dynamical techniques for downscaling local climate. J. Climate **12**, 2256–2284 (1999)
12. Bennet, A.: Inverse Methods in Physical Oceanography, p. 346. Cambridge University Press, Cambridge, UK (1992)
13. Altaf, M.U., Butler, T., Mayo, T., Luo, X., Dawson, C., Heemink, A.W., Hoteit, I.: A comparison of ensemble Kalman filters for storm surge assimilation. Mon. Wea Rev. **142**, 2889–2914 (2014)
14. Altaf, M.U., Ambrozic, M., McCabe, M.F., Hoteit, I.: A study of reduced-order 4DVAR with a finite element shallow water model. Int. J. Numer. Methods Fluids **80**, 631–647 (2016)
15. Charney, J., Halem, J., Jastrow, M.: Use of incomplete historical data to infer the present state of the atmosphere. J. Atmos. Sci. **26**, 1160–1163 (1969)
16. Daley, R.: Atmospheric Data Analysis. Cambridge Atmospheric and Space Science Series, Cambridge University Press, Cambridge (1991)
17. Henshaw, W.D., Kreiss, H.O., Ystrom, J.: Numerical experiments on the interaction between the large and small scale motion of the Navier Stokes equations. SIAM J. Multiscale Modeling Simulation **1**, 119–149 (2003)
18. Olson, E., Titi, E.S.: Determining modes for continuous data assimilation in 2D turbulence. J. Stat. Phys. **113**, 799–840 (2003)
19. Olson, E., Titi, E.S.: Determining modes and Grashoff number in 2D turbulence. Theor. Comput. Fluid Dyn. **22**, 327–339 (2009)
20. Korn, P.: Data assimilation for the Navier-Stokes-α equations. Physica D **238**, 1957–1974 (2009)
21. Hayden, K., Olson, E., Titi, E.S.: Discrete data assimilation in the Lorenz and $2D$ Navier–Stokes equations. Physica D **240**, 1416–1425 (2011)

22. Azouani, A., Olson, E., Titi, E.S.: Continuous data assimilation using general interpolant observables. J. Nonlinear Sci. **24**, 277–304 (2014)
23. Bessaih, H., Olson, E., Titi, E.S.: Continuous assimilation of data with stochastic noise. Nonlinearity **28**, 729–753 (2015)
24. Farhat, A., Lunasin, E., Titi, E.S.: Abridged continuous data assimilation for the 2D Navier-Stokes equations utilizing measurements of only one component of the velocity field. J. Math. Fluid Mech. **18**, 1–23 (2016)
25. Farhat, A., Lunasin, E., Titi, E.S.: Data assimilation algorithm for 3D Bénard convection in porous media employing only temperature measurements. J. Math. Anal. Appl. **438**, 492–506 (2016)
26. Gesho, M., Olson, E., Titi, E.S.: A computational study of a data assimilation algorithm for the two-dimensional Navier–Stokes equations. Communications in Computational Physics **19**, 1094–1110 (2016)
27. Farhat, A., Jolly, M.S., Titi, E.S.: Continuous data assimilation for the 2D Bénard convection through velocity measurements alone. Phys. D **303**, 59–66 (2015)
28. Ghil, M., Shkoller, B., Yangarber, V.: A balanced diagnostic system compatible with a barotropic prognostic model. Mon. Wea. Rev. **105**, 1223–1238 (1977)
29. Ghil, M., Halem, M., Atlas, R.: Time-continuous assimilation of remote-sounding data and its effect on weather forecasting. Mon. Wea. Rev. **106**, 140–171 (1978)
30. Hoke, J., Anthes, R.: The initialization of numerical models by a dynamic relaxation technique. Mon. Wea. Rev. **104**, 1551–1556 (1976)
31. Aswatha, C.J., Gowda, G., Sridhara, S.N., Seetharamu, K.N.: Buoyancy driven heat transfer in cavities subjected to thermal boundary conditions at bottom wall. Journal of Applied Fluid Mechanics **5**, 43–53 (2012)